

DOI: 10.1002/((please add manuscript number))

Article type: Communication

Direct bandgap behaviour in Rashba-type metal halide perovskites

Johannes M. Richter, Kai Chen, Aditya Sadhanala, Justinas Butkus, Jasmine P.H. Rivett, Richard H. Friend, Bartomeu Monserrat, Justin M. Hodgkiss and Felix Deschler**

Dr. J. M. Richter, Dr. A. Sadhanala, Dr. J. P.H. Rivett, Prof. R. H. Friend, Dr. B. Monserrat, Dr. F. Deschler
Cavendish Laboratory, University of Cambridge, J J Thomson Avenue, Cambridge CB3 0HE, UK
E-mail: fd297@cam.ac.uk

Dr. K. Chen, J. Butkus, Dr. J. M. Hodgkiss
MacDiarmid Institute for Advanced Materials and Nanotechnology, New Zealand
&
School of Chemical and Physical Sciences, Victoria University of Wellington, New Zealand
E-mail: Justin.Hodgkiss@vuw.ac.nz

Keywords: perovskites, ultrafast photoluminescence, direct bandgap, semiconductors

The generation and recombination of charge carriers in semiconductors through photons control photovoltaic and LED operation. Understanding of these processes in hybrid perovskites has advanced, but remains incomplete. Using femtosecond transient absorption and photoluminescence, we observe that the luminescence signal shows a rise over 2 picoseconds, while initially hot photo-generated carriers cool to the band edge. This indicates that the luminescence from hot carriers is weaker than that of cold carriers, as expected from strongly-radiative transitions in direct gap semiconductors. We conclude that the electrons and holes show strong overlap in momentum space, despite recent proposals that Rashba splitting leads to a band offset suppressing such overlap. We consider a number of possible resolutions to this, including lattice dynamics that remove the Rashba splitting at room temperature, and localization of luminescence events to length scales below 10 nm.

Power conversion efficiencies in hybrid perovskite optoelectronic applications now exceed 22% in solar cells^[1] and external quantum efficiencies are above 10% for light-emitting diodes.^[2] The optical properties of these solution-processed poly-crystalline materials show sharp absorption onsets,^[3] comparable to melt-grown crystalline semiconductors, high photoluminescence yields^[4], and low defect densities.^[5] In optoelectronic applications, the carrier lifetime and the band structure of electronic states of a semiconductor ultimately define the performance limits. In particular, high radiative yields are crucial for efficient performance of semiconductors in optoelectronic devices: photon recycling,^[6] which relies on high luminescence yields, has proven to be central to boost photovoltaic efficiencies.^[7]

Recently, results from first principle calculations proposed the potential indirect nature of the band structure of hybrid perovskites.^[8–11] Using density-functional theory, these reports have shown that members of the hybrid perovskite family with non-centrosymmetric crystal structure give rise to a Rashba or Dresselhaus splitting at the band edge. Such calculations are mostly performed for a frozen crystal lattice at 0 K, and without the presence of excited states in the system. The resulting indirect bandgap was predicted to slow down recombination by a factor of ~ 300 ^[9,12]. Experimental reports on angular-resolved photoelectron spectroscopy^[13] have shown first evidence for a Rashba-type band structure in low-temperature phases of bromide perovskites at 4 K, while time-resolved microwave conductivity measurements have found temperature-activated bimolecular recombination.^[14] The latter study is, however, in conflict to an earlier publication by Milot et al. that reports an increase of the bimolecular constant at lower temperatures.^[15] Hot photoluminescence has been used to study carrier relaxation in perovskites with recent reports on polaron formation^[16] and carrier cooling.^[17] However, while some understanding on the recombination dynamics has been gained,^[6,18–21] unambiguous evidence is missing to clarify whether a band structure with indirect or direct optical gap controls the carrier properties and dynamics at room temperature.

The samples used in this work were prepared using standard fabrication procedures^[22] as described in the Experimental section with a thickness of about 150 nm and typical grain sizes of 100s of nm. Sample characterization data, including photothermal deflection absorption measurements, can be found in reference 20.

We use a combination of ultrafast broadband transient absorption (TA) and photoluminescence (PL) spectroscopy to study the early-time carrier relaxation and recombination of perovskites. The combination of these two techniques allows us to study the position of electrons and holes relative to each other in k-space. Whilst TA is sensitive to the sum of electron and hole population, PL measures the overlap and therefore the product of electron and hole carrier distribution for each k-vector, since the presence of both carrier types is required for radiative recombination.

The PL measurements are based on a transient grating method established by Chen et al.^[23], allowing for measuring spectrally-resolved PL with low background noise and ~200-fs resolution. Due to the long carrier lifetimes of perovskites, a low background level is crucial for studying the sub-picosecond luminescence. **Figure 1A and 1B** show the early-time PL maps of hybrid lead bromide and iodide perovskite, respectively, which are centered around the band edge at 535 nm for bromide and 770 nm for iodide perovskite. In contrast to transient absorption, where a distinguished hot carrier population has been reported^[17,24] (see also Figure S1), the PL only shows a weak hot carrier emission above the band edge. **Figure 1C** shows the PL intensity after the initial rise (PL^{\max}) at 1.5 ps after excitation, as a function of pump fluence. The peak PL intensity scales quadratically with pump fluence, indicating that this early-time PL originates from band-to-band bimolecular recombination of carriers rather than excitonic recombination. **Figure 2A** shows the TA spectra and PL spectra for the

bromide perovskite. The TA spectra at early times show a clear contribution from hot carriers at wavelengths shorter than 515 nm (energies higher than 2.4 eV) which cool to longer wavelengths (lower energies) over time, as seen by the rise of the TA signal near the band edge (525 – 550 nm) and the simultaneous decay of the hot carriers. This carrier cooling can be quantified by determining the carrier temperature from TA spectra via fitting to Boltzmann functions to the high-energy tail of the photo-bleach according to ^[24]

$$\frac{\Delta T}{T}(E) \sim \exp\left(-\frac{E - E_f}{k_B T_C}\right) \quad (1)$$

where k_B denotes the Boltzmann constant and E_f the Fermi energy. We fit equation (1) to the high-energy tail of the TA spectra and extract the time-dependent carrier temperature. We note that this is an estimate for the average temperature of electrons and holes, although it is likely that both are similar due to similar effective masses of the band states ^[9] and due to sub-100 fs energy exchange via carrier-carrier scattering ^[25].

In contrast to the TA spectra, the PL spectra do not show strong contribution from hot carriers (see Figure S7 and S8 for normalised PL spectra). Most of the PL in the wavelength region shorter than 515 nm is due to phonon broadening ^[26]. Instead, the PL spectra show a constant rise whilst the TA spectra show carrier cooling. This suggests that PL emission of a hot carrier population is weaker than emission from carriers concentrated at the band edge. **Figure 2B and 2C** show the spectrally-integrated PL kinetics for the bromide perovskite. We observe a rise-time longer than the setup response function. Moreover, the rise-time is significantly longer than the sub-50 fs timescales measured for dephasing and thermalization. ^[25,27] The picosecond PL rise-time is in very good agreement with the rise of the TA bleaching signal at the band edge energy and thus with the rise of the cold carrier population as seen in Figure 2C. Consistent with the dominance of PL from the band edge, the PL rise time is shortened to 205 fs when exciting the bromide perovskite closer to the band edge, at 500 nm (Figure 2B).

Furthermore, the PL rise gets longer at high fluences where a hot phonon effect delays carrier cooling^[24] as seen by the slower rise in the cold carrier TA signal in Figure 2C. This confirms that carrier recombination of cold carriers is stronger than that of hot carriers.

We measure the photoluminescence rise for the iodide perovskite and observe a rise over 2 ps (**Figure 3A**), again, much slower than the setup response (275 fs for experiments on iodide perovskites). We show below that such observations are not in agreement with strong effects on recombination from an indirect bandgap in perovskites. These were theoretically predicted in bandstructure calculations due to a strong spin-orbit coupling and experimental results from photoelectron spectroscopy have been presented^[8,10,11,13]. Several recent reports invoke an indirect bandgap as a reason for potentially slow radiative recombination in perovskites^[9,11,14,28]. We use the indirect bandstructure calculations by the Schilfgaarde group^[9] to model transient PL kinetics based on a Fermi-Dirac state-filling model, and the extracted carrier temperatures from our experimental TA (see Figure 3A). Details of the model can be found in Suppl. Note 2. We plot the modelled time-dependent PL emission together with the experimental PL kinetic in Figure 3A for the iodide perovskite. In strong contradiction to the experimental data, which shows a rise of the PL emission over 2 ps, the indirect bandgap model predicts a fast decay of PL emission, as in an indirect bandgap picture, cold carrier emission from k-mismatched carriers would be less efficient than early-time emission from hot carriers. For comparison, we also model the PL kinetic for the same bandstructure but with a shifted valence band in order to make the bandgap direct. We observe an excellent agreement of this direct bandgap model with our experimental data in Figure 2C. In this model, the stronger PL emission at the band edge results from the higher concentration of k-matched carriers at that energy, rather than a higher intrinsic radiative rate. Hot PL is not forbidden, rather it is weak as result of the distribution of k-matched carriers. This suggests

that the PL behavior of perovskite is better described with a direct bandgap model, rather than an indirect one.

We also compute the PL dynamics for different band offsets in Figure S3B. We find that a small band offset of 20% or less of the indirect band model of Azarhoosh et al.^[9] gives PL dynamics very similar to the direct bandgap ones. Therefore, such a small band offset results in quasi-direct bandgap behaviour and PL emission is not thermally activated anymore. At the experimental fluences used in this work, band-filling effects play a minor role as seen in Figure S3A. Similar to Azarhoosh et al.^[9], we find that band-filling effects only become dominant at fluences above 10^{18}cm^{-3} .

Radiative recombination in bulk hybrid perovskites was reported^[4,15] to originate from bimolecular recombination, following the formula $\frac{dn}{dt} = -b_{rad} \cdot n^2$, with carrier density n . We plot the bimolecular constant b_{rad} as a function of carrier temperature in **Figure 3B** to study the thermal activation of the PL. We extract the time-dependent carrier temperature from Boltzmann-fits to the band-edge bleach signal in TA measurements^[24]. The total PL emission, which is a relative measure of b_{rad} , is plotted over carrier temperature, with time as the implicit variable. We observe that the bimolecular constant decreases with increasing carrier temperature, and that therefore, PL emission in perovskites is not thermally activated. This is in contrast to expected behavior from recombination of a strongly indirect bandgap. In Figure 3B, we also plot theoretical predictions for the bimolecular constant under an indirect bandgap as computed by Azarhoosh et al.^[9]. The temperature dependence deviates from our experimental data significantly. Moreover, we find a good agreement of our experimental data with a direct bandgap model.

In order to investigate the effect of lattice temperature on PL emission, we perform temperature-dependent PL measurements. Figure S4 shows the time-integrated PL emission intensity as a function of fluence for different temperatures for iodide and bromide perovskite as a relative measure for PLQEs. We observe that the PL emission is stronger at lower temperatures by up to one order of magnitude. Our data shows no evidence for a temperature activation of PL emission. The increase of PL emission at low temperatures agrees with trap deactivation and an increase of the bimolecular constant b_{rad} as shown in Figure 3B, and as reported for seminal crystalline semiconductors. We note that crystal phase transitions are occurring at low temperatures in both iodide and bromide perovskite [15,29–31]. We performed measurements for iodide perovskite at 180 K, just above the phase transition, which shows that the PL intensity increases at lower temperature within the same crystal phase. However, the detailed effects of phase transitions are not relevant for the focus of this study.

We report a rise in PL intensity during carrier cooling as well as an increase of PL emission at low temperatures in hybrid perovskites. We therefore conclude that PL emission in these materials is not temperature-activated and that there is no significant slow-down of PL emission rates due to an indirect bandgap. Electrons and holes appear as if they have strong overlap in k-space. This is in contrast to theoretical predictions from recent reports,^[8–11] which predict a significant temperature activation of PL emission based on bandstructure calculations, which include a Rashba-like bandgap splitting. Whilst our data shows that PL emission is not affected by an indirect bandgap, we cannot fully rule out the presence of a very small indirect bandgap as modeled in Figure S3B. However, the offset must be smaller than the theoretically proposed one in order to match our experimental results, which show that electrons and holes strongly overlap in k-space.

The discrepancy between our direct experimental results and the theoretical predictions might have different origins. The clearest difference is that whilst most of the reported band structures are computed for 0 K, our experiment is performed at room temperature, where thermal lattice dynamics and molecular rotations are present. Electron-phonon coupling has been reported to broaden the PL peak to 120 meV in iodide perovskite at 300 K^[26] and is expected to perturb the calculated band structures. To confirm this, we have performed finite temperature density functional theory calculations^[32,33] of the band structures of the bromide and iodide hybrid perovskites (see Supplementary Note 3 [for computational details](#)). We find that the thermal energy associated with lattice dynamics is comparable to the Rashba splitting of the band edges, and the finite temperature band structures do not exhibit significant indirect gaps, as seen in **Figure 4** (see Figure S5 and S6 for full band structure). Furthermore, molecular rotations render the average structure centrosymmetric, leading to a dynamical spin splitting^[34] in which the bands have no definite spin texture. A second potential origin for the discrepancy with earlier theories is a large uncertainty in the k-vector of charge carriers due to a spatially limited extension of the electron wavefunction. This would be in agreement with the observation of quantum confinement in perovskite nanocrystals, which only occurs for sizes smaller than 10 nm, which suggest that this is in the order of the size of the charge wavefunctions. This length-scale would translate to an uncertainty in k-vector of about 7 % of the Brillouin zone, at which offsets between reported indirect bandgaps would become irrelevant.

In contrast to our observation of a decrease of the radiative bimolecular constant b_{rad} with temperature, Hutter et al. recently reported an increase of the bimolecular constant with temperature^[14]. In these measurements, the bimolecular constant was extracted from time-resolved photoconductivity measurements. Notably, these bimolecular constants were at least one order of magnitude larger than reports from other groups^[18,20,35]. As recently reported by

our group, there is evidence for a non-radiative contribution to the bimolecular constant, which is likely to be connected to trap assisted recombination^[20,36]. It is therefore likely that the temperature dependence observed by Hutter et al. is due to trap deactivation rather than a change in the radiative part of the bimolecular constant. In our present study we avoid this problem, since we are using time-resolved PL as a measure for the bimolecular constant prior the timescale of any trapping and detrapping. Thus, we are only measuring the radiative component of the bimolecular constant and are not affected by any other recombination pathway. Furthermore, the reports by Hutter et al. and Wang et al. rely on multi-parameter fitting of a recombination model^[12,14] whilst our experiment tracks the bimolecular constant directly and relies on no modelling assumptions. Therefore, our reported changes in the bimolecular constant reflect the direct change in the band-to-band recombination of free electrons and holes. Niesner et al. have reported experimental evidence for a Rashba effect in bromide perovskites at low temperatures using surface-sensitive angular-resolved photoelectron spectroscopy.^[13] In connection with our data, this indicates that strong Rashba effects might only be observed at low temperatures and that lattice dynamics reduces the band extrema splitting at room temperature, as recently reported in other Rashba materials.^[37]

We have shown that photoluminescence emission in hybrid perovskites is not slowed down by an indirect bandgap. This result is crucial for understanding the remarkable device performance of perovskites: Only semiconductors that behave like direct bandgap semiconductors allow for efficient electroluminescence in light-emitting diodes. Furthermore, lasing would only be possible once band filling effects allow stimulated emission, which will only occur at fluences higher than 10^{20} cm^{-3} in an indirect semiconductor, as calculated in Figure S3A. This is in contrast to the hybrid perovskites where lasing has been observed at fluences of 10^{18} cm^{-3} . For solar cells, indirect bandgap effects have been invoked as beneficial by suppressing charge recombination rates^[14,38]. We note firstly that the bimolecular

recombination constants for perovskites are in fact not low; the bimolecular recombination constant we resolve for perovskites are comparable to the prototypical high mobility direct bandgap semiconductor, GaAs^[39] and Langevin theory is not an appropriate model for either of these materials, since recombination is not mobility-limited. Secondly, strong band edge emission is highly beneficial not only for efficient LED, but also solar cell operation: For a given trap density, high open-circuit voltages are obtained for high PLQEs, that is, when radiative recombination outcompetes non-radiative channels.^[6,7,40]

Experimental Section

Film preparation: For the iodide perovskite films, 3:1 molar stoichiometric ratios of CH₃NH₃I (CH₃NH₃Br for bromide perovskite) and Pb(CH₃COO)₂ (Sigma Aldrich 99.999% pure) were made in N,N-dimethylformamide (DMF) in 20 wt% solution. This solution was spun inside a nitrogen filled glove box on quartz substrates at 2,000 r.p.m. for 60 s followed by 3 min of thermal annealing at 100 °C in air to form thin films. The samples were encapsulated with a second glass slide and epoxy adhesive (Loctite Double Bubble) under inert conditions to avoid sample degradation and beam damage.

Transient grating PL setup: We used two different laser systems for the bromide and iodide perovskite samples. For the bromide perovskite, a Ti:Sapphire amplifier system (Spectra-Physics Solstice) operating at 1 KHz generating 80-fs pulses was split into the pump and probe beam arms. The pump beam was generated by second harmonic generation (SHG) in a BBO crystal and focused onto the sample. Photoluminescence is collimated using a silver off-axis parabolic mirror and focused onto the gate medium. About 80 μJ/pulse of the 800 nm laser output is used for the gate beams, which is first raised 25 mm above the plane of the PL

to produce a boxcar geometry and split into a pair of gate beams using a 50/50 beam splitter. The gate beams are focused onto the gate medium (fused silica), crossing at an angle of $\sim 5^\circ$ and overlapping with the focused PL. The two gate beams interfere and create a transient grating in the gate medium due to a modulation of the refractive index via the optical Kerr effect ^[23]. Temporal overlap between the two gate beams is achieved via a manual delay stage. The PL is then deflected on the transient grating causing a spatial separation of the gated signal from the PL background. Two lenses collimate and focus the gated signal onto the spectrometer entrance (Princeton Instruments SP 2150) after long- and short-pass filters remove scattered pump and gate light, respectively. Gated PL spectra are measured using an intensified CCD camera (Princeton Instruments, PIMAX4). The (~ 10 ns) electronic shutter of the intensified CCD camera was used to further suppress long-lived PL background. PL spectra at each gate time delay are acquired from $\sim 10\,000$ laser shots. The time delay between pump and gate beams is controlled via a motorized optical delay line on the excitation beam path and a LabVIEW data acquisition program.

Because the redder PL spectrum of the iodide sample overlaps with the fundamental output of a Ti:Sapphire laser, we used the 1030 nm output of Yb fibre laser (Amplitude Systèmes, Tangerine) operating at 100 kHz. The fibre laser was modified to provide compressed pulses of <150 fs duration. A fraction of this beam was frequency-doubled to generate a 515 nm pump, with $40\ \mu\text{J}/\text{pulse}$ of the fundamental 1030 nm used to generate the pair of gate beams. The ultrafast PL spectrometer is the essentially same as described above for the Ti:Sapphire system, with the following differences. The gate beam path used HR dielectric mirrors at 1030 nm for the high average power laser output. A 2-mm undoped Yttrium aluminium garnet crystal was used as the gate medium. The FWHM of the instrument response function of the system is about 230 fs. The transient PL spectra were resolved by a polychromator equipped with a spectrometer (SP 2150) and low temperature camera fitted with a Hamamatsu S10140-1108 sensor. This system also benefits from the higher signal to noise associated with a higher

repetition rate by accumulating 200 000 laser shots in 2 seconds exposure time for a single spectrum at each time step.

Transient absorption spectroscopy: A Ti:Sapphire amplifier system (Spectra-Physics Solstice) operating at 1 KHz generated 90-fs pulses was split to given the pump and probe beam arms. The broad band probe pulses were generated in a home-built non-collinear optical parametric amplifier. The pulsed excitation was provided by a TOPAS optical parametric amplifier (Light Conversion), to generate narrowband (10 nm full-width at half-maximum) pump pulses of 490 nm for bromide perovskite samples and 650nm for iodide and iodide-chloride perovskite samples. The transmitted pulses were collected with an InGaAs dual-line array detector (Hamamatsu G11608-512) driven and read out by a custom-built board from Stresing Entwicklungsbüro.

Supporting Information

Supporting Information is available from the Wiley Online Library or from the author.

Acknowledgements

We acknowledge financial support from the Engineering and Physical Sciences Research Council of the UK (EPSRC). J.M.R. thank the Winton Programme for the Physics of Sustainability (University of Cambridge). J.M.R. thanks the Cambridge Home European Scheme for financial support. B.M thanks Robinson College and the Cambridge Philosophical Society for a Henslow Research Fellowship. F.D. acknowledges funding from a Herchel Smith Research Fellowship and a Winton Advanced Research Fellowship. K.C., J.B, and J.M.H. gratefully acknowledge Yoann Zaouter, Florent Guichard (Amplitude Systèmes), and Loïc Lavenu (Amplitude Systèmes and Institut d'Optique, CNRS, Université Paris Saclay) for providing access and assistance with the Amplitude Systèmes laser used for ultrafast PL measurements. We thank Michael Price for providing support in setting up the band-filling model. The experimental data that support the findings of this study are available in the University of Cambridge Repository (<https://www.repository.cam.ac.uk/>).

Received: ((will be filled in by the editorial staff))

Revised: ((will be filled in by the editorial staff))

Published online: ((will be filled in by the editorial staff))

References

- [1] W. S. Yang, B.-W. Park, E. H. Jung, N. J. Jeon, Y. C. Kim, D. U. Lee, S. S. Shin, J. Seo, E. K. Kim, J. H. Noh, S. Il Seok, *Science* **2017**, *356*, 1376.
- [2] W. Peng, J. Yin, K. Ho, O. Ouellette, M. De Bastiani, B. Murali, O. El Tall, C. Shen, X. Miao, J. Pan, E. Alarousu, J. He, B. S. Ooi, O. F. Mohammed, E. Sargent, O. M. Bakr, *Nano Lett.* **2017**, *17*, 4759.
- [3] A. Sadhanala, F. Deschler, T. H. Thomas, S. E. Dutton, K. C. Goedel, F. C. Hanusch, M. L. Lai, U. Steiner, T. Bein, P. Docampo, D. Cahen, R. H. Friend, *J. Phys. Chem. Lett.* **2014**, *5*, 2501.
- [4] F. Deschler, M. Price, S. Pathak, L. E. Klintberg, D.-D. D. Jarausch, R. Higler, S. Hüttner, T. Leijtens, S. D. Stranks, H. J. Snaith, M. Atatüre, R. T. Phillips, R. H. Friend, *J. Phys. Chem. Lett.* **2014**, *5*, 1421.
- [5] D. W. deQuilettes, S. Koch, S. Burke, R. K. Paranjli, A. J. Shropshire, M. E. Ziffer, D. S. Ginger, *ACS Energy Lett.* **2016**, *1*, 438.
- [6] L. M. Pazos-Outón, M. Szumilo, R. Lamboll, J. M. Richter, M. Crespo-Quesada, M. Abdi-Jalebi, H. J. Beeson, M. Vrućinić, M. Alsari, H. J. Snaith, B. Ehrler, R. H. Friend, F. Deschler, *Science* **2016**, *351*, 1430.
- [7] R. T. Ross, *J. Chem. Phys.* **1967**, *46*.
- [8] F. Brivio, K. T. Butler, A. Walsh, M. van Schilfgaarde, *Phys. Rev. B* **2014**, *89*, 155204.
- [9] P. Azarhoosh, S. McKechnie, J. M. Frost, A. Walsh, M. van Schilfgaarde, *APL Mater.* **2016**, *4*, 91501.
- [10] T. Etienne, E. Mosconi, F. De Angelis, *J. Phys. Chem. Lett.* **2016**, *7*, 1638.
- [11] F. Zheng, L. Z. Tan, S. Liu, A. M. Rappe, *Nano Lett.* **2015**, *15*, 7794.
- [12] T. Wang, B. Daiber, J. M. Frost, S. A. Mann, E. C. Garnett, A. Walsh, B. Ehrler, *Energy Environ. Sci.* **2017**, *10*, 509.
- [13] D. Niesner, M. Wilhelm, I. Levchuk, A. Osvet, S. Shrestha, M. Batentschuk, C. Brabec, T. Fauster, *Phys. Rev. Lett.* **2016**, *117*, 126401.

- [14] E. M. Hutter, M. C. Gélvez-Rueda, A. Osherov, V. Bulović, F. C. Grozema, S. D. Stranks, T. J. Savenije, *Nat. Mater.* **2016**, *16*, 115.
- [15] R. L. Milot, G. E. Eperon, H. J. Snaith, M. B. Johnston, L. M. Herz, *Adv. Funct. Mater.* **2015**, *25*, 1.
- [16] K. Miyata, D. Meggiolaro, M. T. Trinh, P. P. Joshi, E. Mosconi, S. C. Jones, F. De Angelis, X.-Y. Zhu, *Sci. Adv.* **2017**, *3*, e1701217.
- [17] K. Chen, A. J. Barker, F. L. C. Morgan, J. E. Halpert, J. M. Hodgkiss, *J. Phys. Chem. Lett.* **2015**, *6*, 153.
- [18] M. B. Johnston, L. M. Herz, *Acc. Chem. Res.* **2016**, *49*, 146.
- [19] M. Saba, M. Cadelano, D. Marongiu, F. Chen, V. Sarritzu, N. Sestu, C. Figus, M. Aresti, R. Piras, A. Geddo Lehmann, C. Cannas, A. Musinu, F. Quochi, A. Mura, G. Bongiovanni, *Nat. Commun.* **2014**, *5*, 5049.
- [20] J. M. Richter, M. Abdi-Jalebi, A. Sadhanala, M. Tabachnyk, J. P. H. Rivett, L. M. Pazos-Outón, K. C. Gödel, M. Price, F. Deschler, R. H. Friend, *Nat. Commun.* **2016**, *7*, 13941.
- [21] T. Kirchartz, F. Staub, U. Rau, *ACS Energy Lett.* **2016**, 731.
- [22] W. Zhang, M. Saliba, D. T. Moore, S. K. Pathak, M. T. Hörantner, T. Stergiopoulos, S. D. Stranks, G. E. Eperon, J. A. Alexander-Webber, A. Abate, A. Sadhanala, S. Yao, Y. Chen, R. H. Friend, L. A. Estroff, U. Wiesner, H. J. Snaith, *Nat. Commun.* **2015**, *6*, 6142.
- [23] K. Chen, J. K. Gallaher, A. J. Barker, J. M. Hodgkiss, *J. Phys. Chem. Lett.* **2014**, *5*, 1732.
- [24] M. B. Price, J. Butkus, T. C. Jellicoe, A. Sadhanala, A. Briane, J. E. Halpert, K. Broch, J. M. Hodgkiss, R. H. Friend, F. Deschler, *Nat. Commun.* **2015**, *6*, 8420.
- [25] J. M. Richter, F. Branchi, F. Valduga de Almeida Camargo, B. Zhao, R. H. Friend, G. Cerullo, F. Deschler, *Nat. Commun.* **2017**, *8*, 376.

- [26] A. D. Wright, C. Verdi, R. L. Milot, G. E. Eperon, M. A. Pérez-Osorio, H. J. Snaith, F. Giustino, M. B. Johnston, L. M. Herz, *Nat. Commun.* **2016**, *7*, 11755.
- [27] S. A. March, D. B. Riley, C. Clegg, D. Webber, X. Liu, M. Dobrowolska, J. K. Furdyna, I. G. Hill, K. C. Hall, *ACS Photonics* **2017**, *4*, 1515.
- [28] Z.-G. Yu, *Phys. Chem. Chem. Phys.* **2017**, *19*, 14907.
- [29] N. Onoda-Yamamuro, T. Matsuo, H. Suga, *J. Phys. Chem. Solids* **1990**, *51*, 1383.
- [30] S. Singh, C. Li, F. Panzer, K. L. Narasimhan, A. Graeser, T. P. Gujar, A. Köhler, M. Thelakkat, S. Huettner, D. Kabra, *J. Phys. Chem. Lett.* **2016**, *7*, 3014.
- [31] F. Panzer, S. Baderschneider, T. P. Gujar, T. Unger, S. Bagnich, M. Jakoby, H. Bäessler, S. Hüttner, J. Köhler, R. Moos, M. Thelakkat, R. Hildner, A. Köhler, *Adv. Opt. Mater.* **2016**, *4*, 917.
- [32] K. Kunc, R. M. Martin, *Phys. Rev. Lett.* **1982**, *48*, 406.
- [33] J. H. Lloyd-Williams, B. Monserrat, *Phys. Rev. B* **2015**, *92*, 184301.
- [34] B. Monserrat, D. Vanderbilt, *Phys. Rev. Mater.* **2017**, *1*, 54201.
- [35] C. Wehrenfennig, G. E. Eperon, M. B. Johnston, H. J. Snaith, L. M. Herz, *Adv. Mater.* **2014**, *26*, 1584.
- [36] F. Staub, T. Kirchartz, K. Bittkau, U. Rau, *J. Phys. Chem. Lett.* **2017**, *8*, 5084.
- [37] B. Monserrat, D. Vanderbilt, *arXiv* **2017**, 1711.06274.
- [38] F. Zheng, L. Z. Tan, S. Liu, A. M. Rappe, *Nano Lett.* **2015**, 151013115142009.
- [39] Y. P. Varshni, *Phys. Status Solidi* **1967**, *19*, 459.
- [40] I. Schnitzer, E. Yablonovitch, C. Caneau, T. J. Gmitter, *Appl. Phys. Lett.* **1993**, *62*, 131.

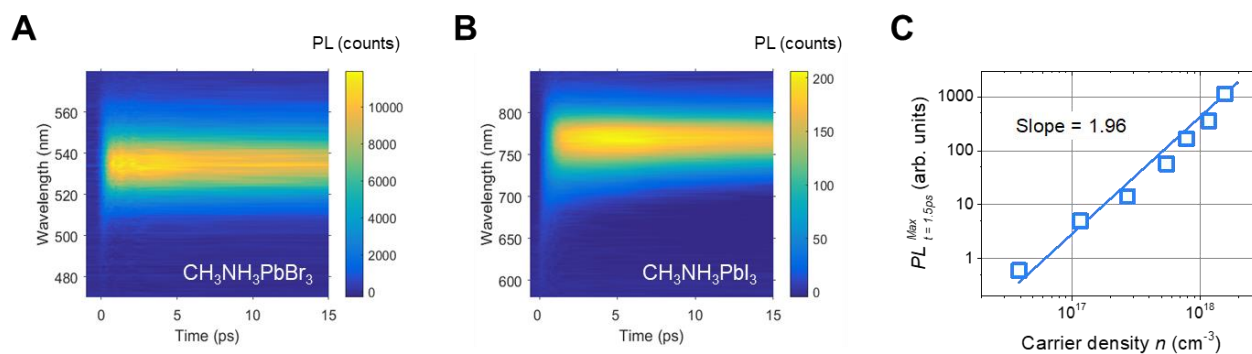


Figure 1: Femtosecond photoluminescence of hybrid perovskites. (A), (B) Transient photoluminescence (PL) map of (A) $\text{CH}_3\text{NH}_3\text{PbBr}_3$ and (B) $\text{CH}_3\text{NH}_3\text{PbI}_3$ at a fluence of $20 \mu\text{J}/\text{cm}^2$ and $7 \mu\text{J}/\text{cm}^2$, respectively. There is no strong contribution to the PL from hot carriers but a strong emission from the bandedge. (C) PL intensity at 1.5 ps after excitation (PL^{max}) plotted over carrier density for $\text{CH}_3\text{NH}_3\text{PbBr}_3$. The PL intensity scales quadratic in carrier density, suggesting that free charge carrier recombination dominates the early-time emission.

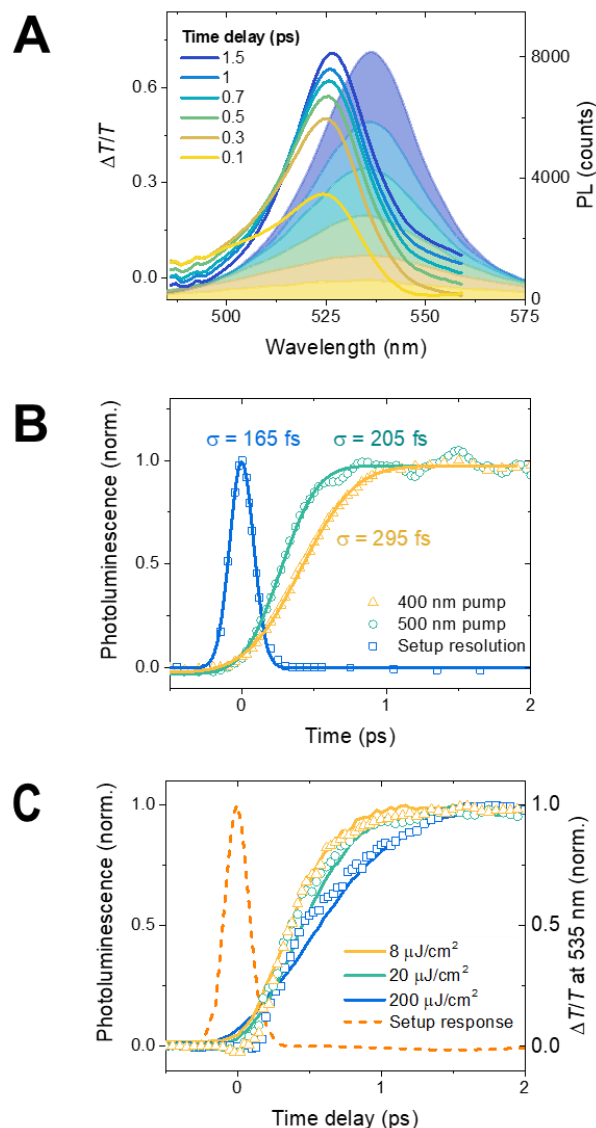


Figure 2: Photoluminescence rise during carrier cooling in $\text{CH}_3\text{NH}_3\text{PbBr}_3$. (A) Transient absorption (TA, continuous lines) and photoluminescence (PL, filled lines) spectra of $\text{CH}_3\text{NH}_3\text{PbBr}_3$ at a fluence of $200 \mu\text{J}/\text{cm}^2$ for different time delays after excitation. Whilst the TA spectra shift to longer wavelengths due to carrier cooling, the PL spectra rise in intensity. (B) PL rise of bromide perovskite for 400 nm (yellow triangles) and 500 nm (green circles) excitation with a fluence of $40 \mu\text{J}/\text{cm}^2$. The band gap is 535 nm. The PL shows a rise slower than the setup response (blue squares). The risetime is longer for the higher energy pump (295 fs for 400nm) compared to the lower energy pump (205 fs for 500nm pump) due to the longer cooling time for the high energy pump. The solid lines represent fits to the data. The setup response was fitted with a Gaussian function and the PL rises were fitted with an error function. (C) PL kinetics (continuous lines) for different fluences for $\text{CH}_3\text{NH}_3\text{PbBr}_3$ pumped at 400 nm. The PL kinetics show a good agreement with TA kinetics (symbols) taken at the red side of the photo-bleach (535 nm) as a measure for the cold carrier population. The rise gets slower at

higher fluences where a hot phonon effect keeps carriers hot for longer. This indicates that the PL rises with the build-up of a cold carrier population. The orange dashed line shows the setup response.

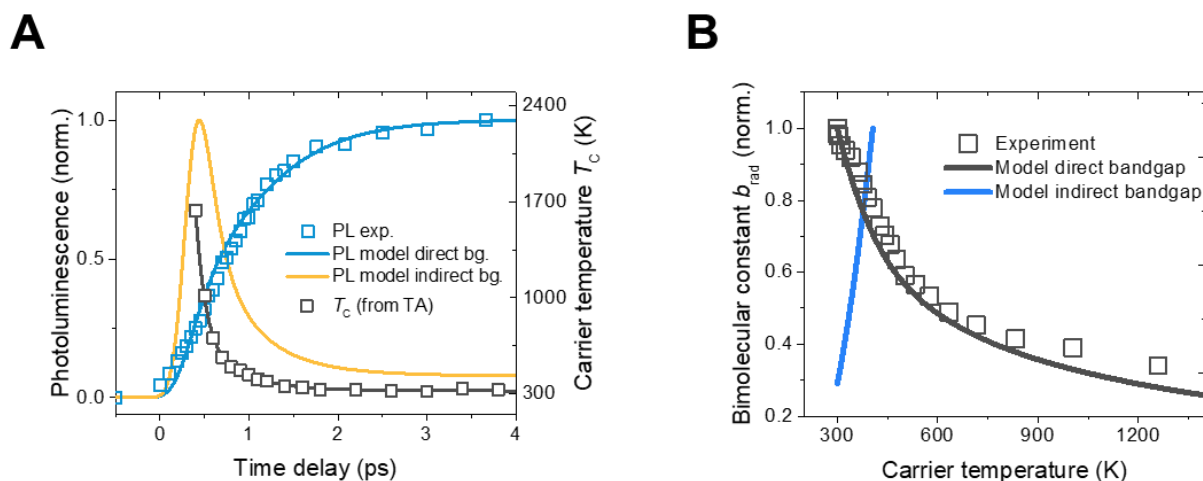


Figure 3: Photoluminescence (PL) rise during carrier cooling in $\text{CH}_3\text{NH}_3\text{PbI}_3$. (a) PL kinetics for $\text{CH}_3\text{NH}_3\text{PbI}_3$ (blue squares). As in $\text{CH}_3\text{NH}_3\text{PbBr}_3$, we observe a rise of PL during carrier cooling. We model the PL kinetics for a **direct (blue line)** and **indirect (yellow line) bandgap** based on calculated bandstructures^[8] using a Fermi-Dirac state-filling model (details in Suppl. Note 2). For an indirect bandgap, the calculations predict a decay when electrons and hole cool to different positions in k-space. For the direct bandgap, we expect a slow rise in signal intensity during carrier cooling due to the narrowing of the Fermi distributions in k-space confining all carriers in a narrow range of k-vectors. (b) Relative radiative bimolecular constant (squares) as a function of carrier temperature for iodide perovskite. The carrier temperature was extracted from transient absorption spectra and the transient PL intensity was taken as a relative measure for the bimolecular recombination constant. Note that time is the implicit variable in the plot. The continuous lines show the modelled radiative bimolecular constant for a direct bandgap model (grey, details in Suppl. Note 2), and for an indirect bandgap model (blue) based on calculations^[9]. Due to the broadening of the carrier Fermi distributions in k-space at high temperatures, the bimolecular constant decreases with increasing temperature for a direct bandgap. For an indirect bandgap, however, this broadening increases the overlap between electron and hole population leading to an increased bimolecular constant, in contradiction to our results.

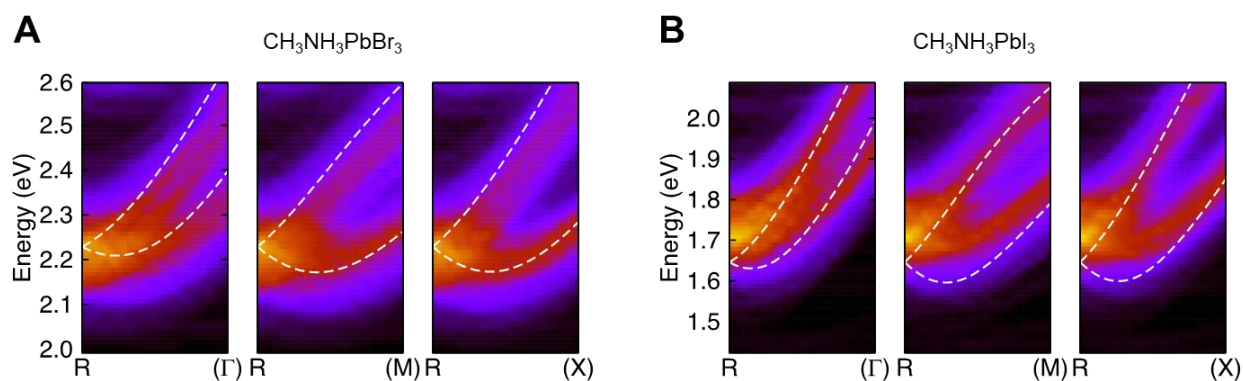


Figure 4: Calculated band structure near the conduction band minimum (CBM) of (A) bromide and (B) iodide perovskite. Density functional theory band structure calculated at the static lattice level (white dashed lines) and at 350 K (contour plots). The band structure is shown along three high-symmetry lines of the pseudo-cubic BZ, starting at the R point where the band gap minimum occurs, and for a distance of 0.25 of the corresponding reciprocal space directions. The CBM shift from the R point present in the static lattice almost completely vanishes at 350 K.

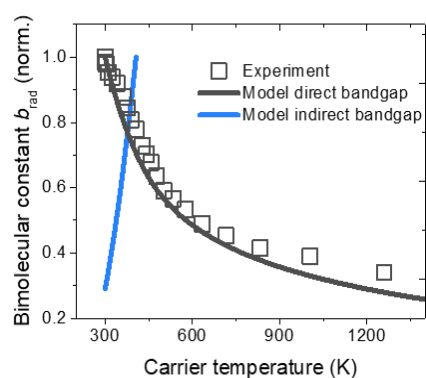
The impact of Rashba effects in perovskite semiconductors is still under debate. Using femtosecond transient absorption and photoluminescence, we show that the luminescence from hot carriers is weaker than that of cold carriers, as expected from strongly-radiative transitions in direct gap semiconductors. We consider a number of possible resolutions to this, including lattice dynamics that remove the Rashba splitting at room temperature.

Metal-halide perovskites, ultrafast photoluminescence, direct bandgap, recombination

J. M. Richter, K. Chen, A. Sadhanala, J. Butkus, J. P.H. Rivett, R. H. Friend, B. Monserrat, J. M. Hodgkiss*, F. Deschler*

Direct bandgap behaviour in Rashba-type metal halide perovskites

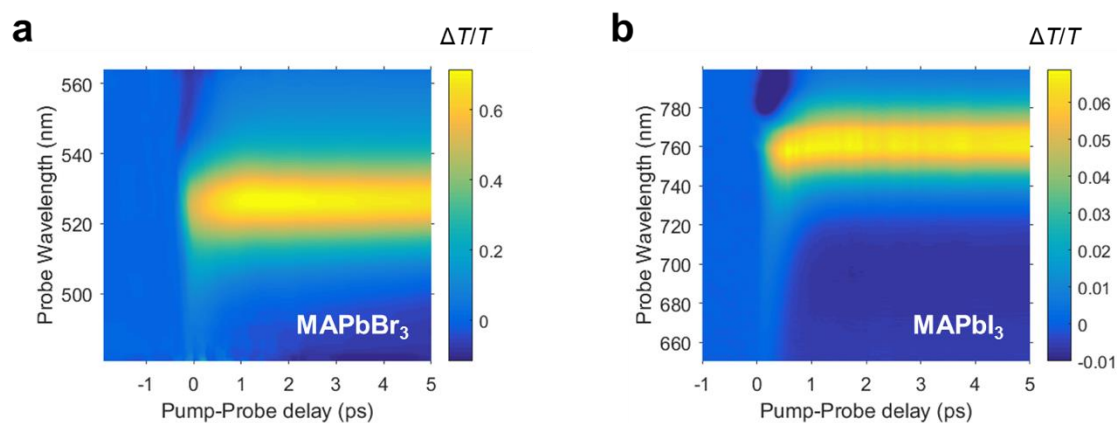
ToC figure



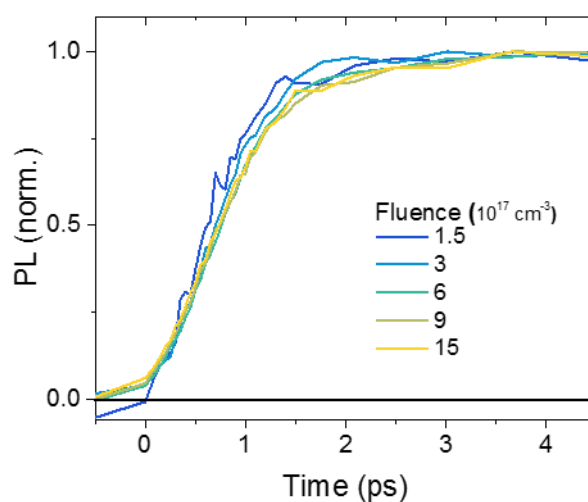
Supporting Information

Direct bandgap behaviour in Rashba-type metal halide perovskites

Johannes M. Richter, Kai Chen, Aditya Sadhanala, Justinas Butkus, Jasmine P.H. Rivett, Richard H. Friend, Bartomeu Monserrat, Justin M. Hodgkiss* and Felix Deschler*

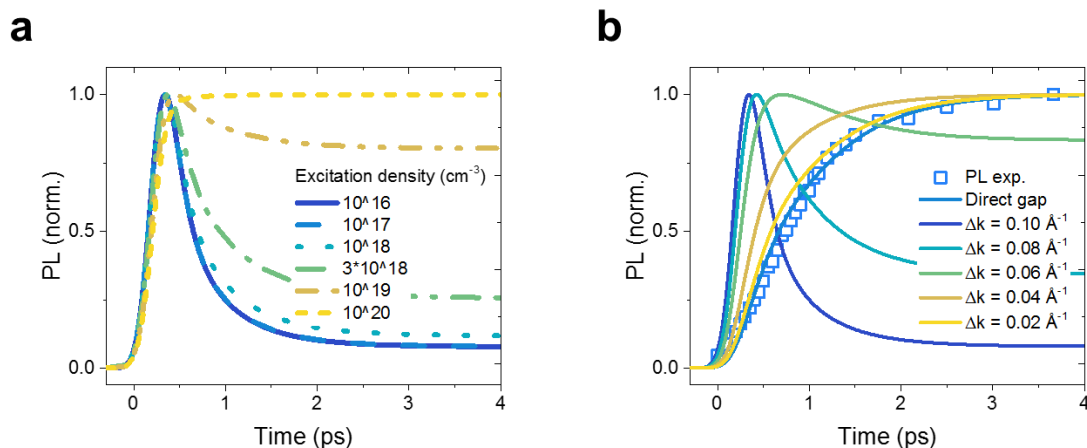
Supplementary Figures

Supplementary Fig. 1: Transient absorption (TA) experiment of hybrid perovskites. (a) - (b) TA data for (a) bromide and (b) iodide perovskite. Initially after photoexcitation, a hot carrier population is formed. During carrier cooling, the carriers exchange energy with the lattice and the population at the bandedge rises.

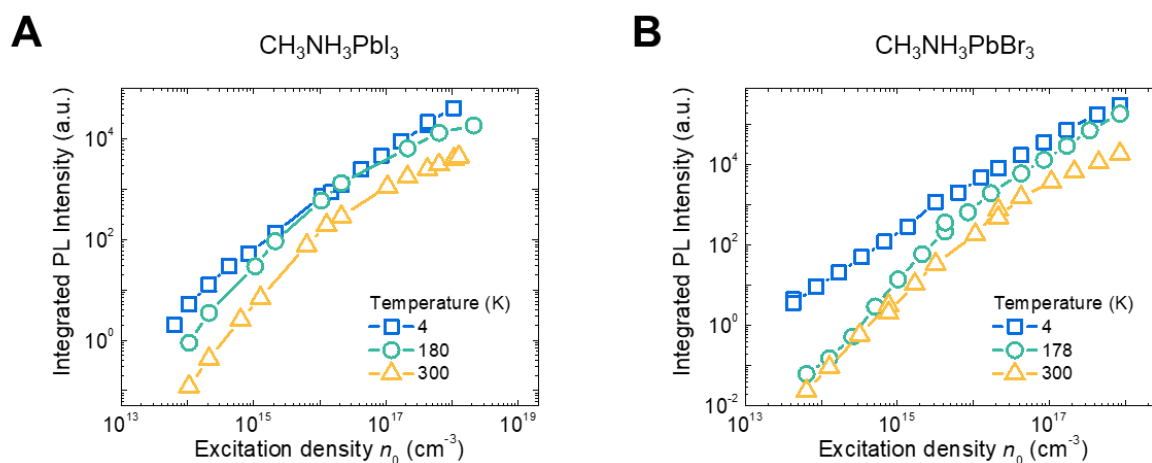


Supplementary Fig. 2: Fluence-dependent photoluminescence (PL) for iodide perovskite.

Fluence-dependent spectrally integrated PL kinetics for iodide perovskites. The kinetics show a rise in PL intensity significantly slower than the setup resolution (about 275 fs). This rise gets slightly longer at higher fluences.

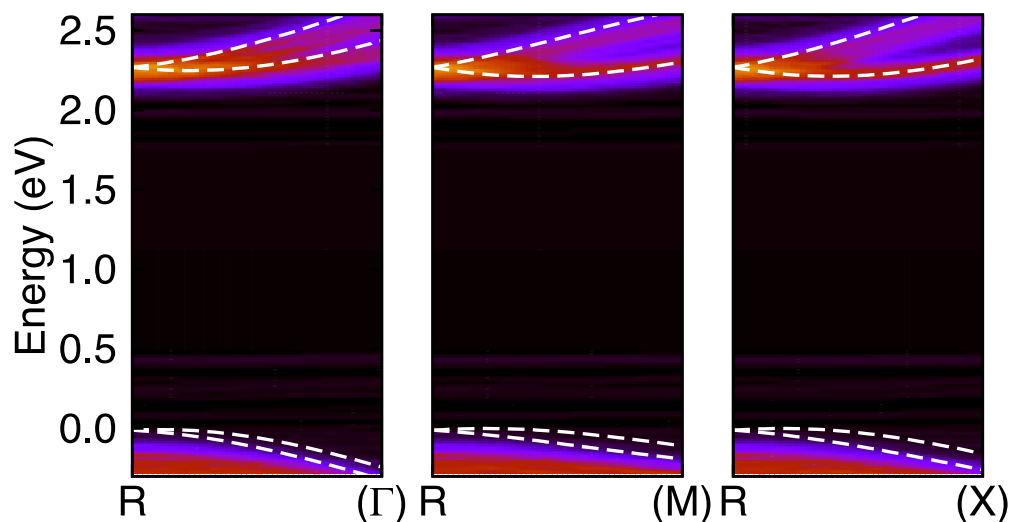


Supplementary Fig. 3: Modelled carrier dynamics for different parameters. (a) Computed carrier dynamics for an indirect bandgap under different excitation densities. Significant bandfilling effects are observed only at fluences higher than 10^{18} cm^{-3} in agreement with calculations by Azarhoosh et al. [7]. (b) Computed carrier dynamics for different shifts Δk of the band extrema relative to each other. Here, $\Delta k = 0.1 \text{ \AA}^{-1}$ represents the behaviour expected from the calculated theoretical band structure [7]. We find that very small indirect bandgaps, where no temperature activation of PL is present anymore, are in agreement with the experimental data.

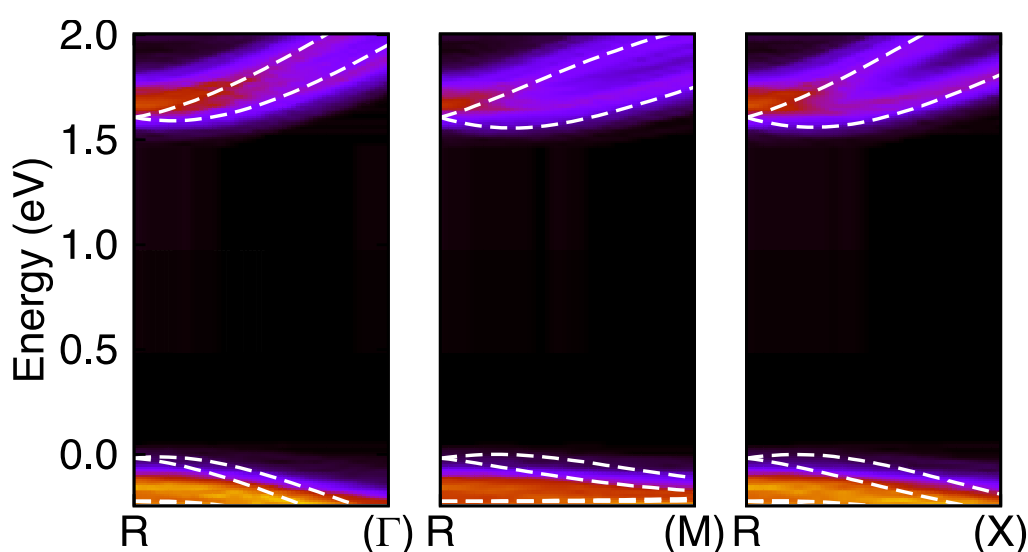
**Supplementary Fig. 4: Temperature-dependent photoluminescence (A) – (B)**

Temperature-dependent time-integrated photoluminescence for (A) $\text{CH}_3\text{NH}_3\text{PbI}_3$ and (B) $\text{CH}_3\text{NH}_3\text{PbBr}_3$ under pulsed excitation. The PL is enhanced by one order of magnitude at low

temperatures, in contrast to an indirect bandgap picture where recombination will be thermally-activated and more efficient at high temperatures.

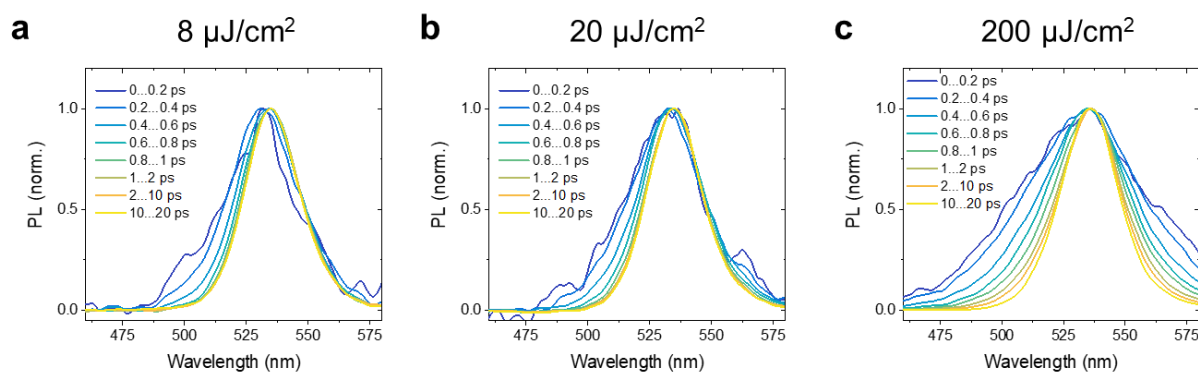


Supplementary Fig. 5: Calculated band structure of the bromide perovskite. Density functional theory band structure calculated at the static lattice level (white dashed lines) and at 350 K (contour plots). The band structure is shown along three high-symmetry lines of the pseudo-cubic BZ, starting at the R point where the band gap minimum occurs, and for a distance of 0.25 of the corresponding reciprocal space directions. The zero of energy is chosen at the valence band maximum, and a scissor operator of 1.24 eV has been applied to correct for the standard semilocal DFT band gap underestimation.

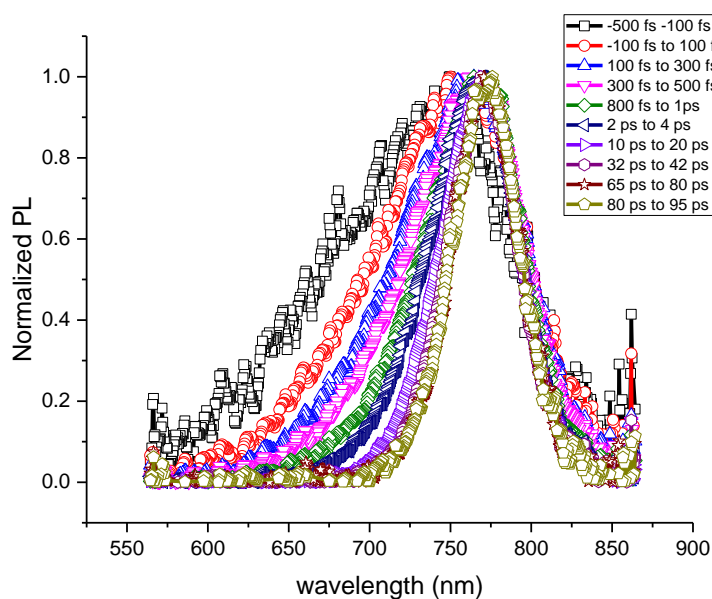


Supplementary Fig. 6: Calculated band structure of the iodide perovskite. Density functional theory band structure calculated at the static lattice level (white dashed lines) and at

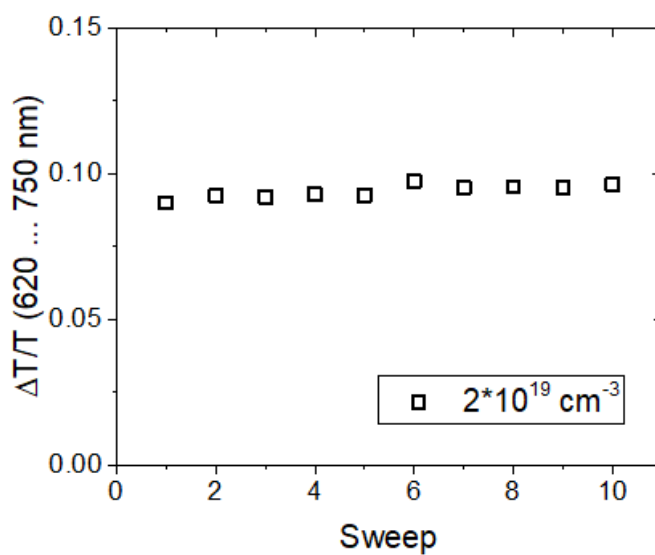
350 K (contour plots). The band structure is shown along three high-symmetry lines of the pseudo-cubic BZ, starting at the R point where the band gap minimum occurs, and for a distance of 0.25 of the corresponding reciprocal space directions. The zero of energy is chosen at the valence band maximum, and a scissor operator of 0.96 eV has been applied to correct for the standard semilocal DFT band gap underestimation.



Supplementary Fig. 7: Normalized PL spectra of bromide perovskite. The normalized PL spectra show a contribution to the PL from hot carriers at early times. At very high fluences (c), a large phonon population causes a strong phonon broadening of the PL at early times.



Supplementary Fig. 8: Normalized PL spectra of iodide perovskite. The normalized PL spectra show a contribution to the PL from hot carriers at early times.



Supplementary Fig. 9: Maximum TA signal of iodide perovskite after the initial rise (at about 1ps) over multiple measurement sweeps. The TA signal is nearly constant over these 10 sweeps indicating that no significant sample degradation has occurred. Each sweep corresponds to about 90 seconds of experimental time.

Supplementary Note 1: Estimate of carrier density

The carrier density n_0 after excitation with a pulsed laser source is estimated using the absorption of the film a , the FWHM of the Gaussian beam d , the laser power P , the laser repetition rate f , the photon energy $E_{\text{ph}} = \hbar\omega$ and the film thickness t . We estimate it as

$$n_0 = \frac{a \cdot P}{E_{\text{ph}} \cdot f} \cdot \frac{1}{\pi(d/2)^2 \cdot t} \quad (2)$$

Supplementary Note 2: Fermi-Dirac carrier model

In order to model the expected photoluminescence dynamics, we performed a Fermi-Dirac state-filling model for the temperature-dependent band occupations of electrons and holes. The electron and hole population probability $\tilde{n}_{e/h}(E)$ is expected to follow a Fermi-Dirac distribution according to

$$\tilde{n}_e(E) = 1 / \left(1 + \exp \left(\frac{E - E_f}{k_B T_C} \right) \right) \quad (3)$$

where E_f denotes the quasi Fermi level, k_B the Boltzmann constant and T_C the carrier temperature. The carrier distribution n_e is then obtained by multiplying the population probability with the density of states which is expected to follow

$$g(k) \propto k^2 \quad (4)$$

The quasi-Fermi level can be approximated by the Nilsson approximation [1] according to

$$E_f = \left(\ln \left(\frac{N}{N_C} \right) + \frac{N}{N_C} \cdot \left[64 + 0.05524 \cdot \frac{N}{N_C} \cdot \left(64 + \sqrt{N/N_C} \right) \right]^{-0.25} \right) k_B T_C \quad (5)$$

where N denotes the excitation density and N_C the effective density of states that can be expressed as [1]

$$N_C = 2 \cdot \left(\frac{m_e k_B T_C}{2\pi\hbar^2} \right)^{\frac{3}{2}} \quad (6)$$

where m_e denotes the effective mass of the carriers. For computing a time-dependent carrier relaxation, the carrier temperature as a function of time was extracted from transient absorption (TA) measurements as seen in Fig. 2c. The carrier density was matched to the experiment using

Supplementary Note 1 to estimate the experimental value. However, as shown in Supplementary Fig. 3, the early-time carrier dynamics are not fluence dependent in this fluence range. The effective masses of the bands was based on bandstructure calculations by the Schilfgaarde group [7] which are in good agreement with reported experimental values [4,8]. The bands were either aligned to form a direct bandgap or with a slight indirect bandgap which was tuned to $\Delta k = 0.1 \text{ \AA}^{-1}$ in order to reproduce the temperature dependent bimolecular constant calculated by Azarhoosh et al. [7]. Since PL emission originates from the overlap of electrons and holes in k space, the PL emission was then calculated according to

$$PL(t) = \int n_e(k, t) \cdot n_h(k, t) dk \quad (7)$$

where n_e and n_h denote the electron and hole distribution functions respectively. We also compute the PL dynamics for different band offsets Δk in Supplementary Fig. 3b. We find that a small band offset of 20% or less of the Azarhoosh band model [7] gives PL dynamics very similar to the direct bandgap ones. Therefore, such a small band offset results in quasi-direct bandgap behaviour and PL emission is not thermally activated.

Supplementary Note 3: Finite temperature band structure

We modelled the band structure of the pseudo-cubic bromide and iodide hybrid perovskites using density functional theory (DFT) [10] in the projector augmented-wave formulation (6) as implemented in the VASP package [12,13]. We used the semilocal exchange-correlation functional of Perdew-Burke-Ernzerhof [14] including the spin-orbit interaction with the second variational method [15]. We chose an energy cut-off of 500 eV and a k -point grid of size $8 \times 8 \times 8$ to sample the electronic Brillouin zone (BZ), with commensurate grids for the supercell calculations.

Our finite temperature calculations were based on the harmonic approximation using the finite displacement method [16] in conjunction with nondiagonal supercells [17]. The vibrational BZ was sampled using a $2 \times 2 \times 2$ q -point grid, and we found quartic dynamical instabilities at the zone boundary M (0.5,0.5,0.0) and R (0.5,0.5,0.5) points of the pseudo-cubic BZ. These instabilities correspond to the known structural phase transitions of the cubic hybrid perovskites to tetragonal and orthorhombic structures upon lowering the temperature. In order to model the pseudo-cubic high temperature phase, we described the unstable phonon modes at the M and R points within the self-consistent harmonic approximation [18], while all other modes were

treated within the standard harmonic approximation. The resulting finite temperature nuclear density was used to stochastically sample configuration space, and for each frozen-phonon configuration an individual band structure calculation was performed.

The static pseudo-cubic structures in our calculations had the methylammonium cations oriented along the $\langle 100 \rangle$ direction. This non-centrosymmetric polar configuration promotes spin splitting as shown by the white dashed lines in Figure S5 and S6, which depict the band structure of the bromide and iodide perovskites around the R point of the pseudo-cubic BZ. In agreement with earlier first principles reports [7,19,20,21], we observe strong spin splitting of the conduction band minima of the hybrid perovskites at the static lattice level, which results in the conduction band minimum shifted from the R point. An enhancement of the photoexcited carrier lifetimes by up to a factor of 300 has been attributed to this offset of the conduction band minimum from the R point [7] and to the spin splitting of the bands [20].

The inclusion of temperature leads to a markedly different picture. The effects of temperature can be divided into two contributions, the faster lattice dynamics and the slower molecular rotations.

The band structure resulting from the inclusion of lattice dynamics (but no molecular rotations) at 350 K is shown as the colour gradients in Figure S5 and S6. The lattice dynamics thermal energy scale is of the same order of magnitude as the spin splitting that appeared at the static lattice level around the band minimum, and as a consequence the finite temperature band structure minimum is no longer shifted, and occurs at the R point. For large k values (sufficiently away from the R point), the energy separation between electronic bands induced by the spin-orbit interaction is larger than the thermal energy scale, and as a consequence the bands remain spin split, like at the static lattice level. We note that the reduction of spin splitting in Rashba systems with increasing temperature has been reported in other materials [22].

The inclusion of molecular cation rotations further modifies the finite temperature band structure, as rotations render the average structure centrosymmetric. For each molecular orientation there will be a preferred direction for the spin splitting, and for opposite molecular orientations the spin splittings will have opposite signs. The resulting physics resembles that of the recently predicted dynamic spin splitting in centrosymmetric crystals [23], with the distinction that the dynamics is driven by the molecular rotations in the hybrid perovskites, whereas it is driven by the optical phonons in standard centrosymmetric crystals.

As a consequence of lattice dynamics and molecular rotations, the finite temperature band structure of the hybrid perovskites shows a direct band gap (Figure S5 and S6) and the energy splitting of the bands exhibits a dynamic spin splitting with both spin orientations contributing

to both bands. Therefore, our analysis predicts that with the combination of lattice vibrations and molecular rotations, both of which occur on timescales shorter than typical carrier lifetimes (of the order of 1 ps for the dynamics compared to multiple ns for the carrier lifetimes), the band structure of the hybrid perovskites behaves like that of a direct band gap semiconductor.

References

- [1] B. R. Bennett, R. A. Soref, and J. A. Del Alamo, *IEEE J. Quantum Electron.* **26**, 113 (1990).
- [2] J. Shah, *Ultrafast Spectroscopy of Semiconductors and Semiconductor Nanostructures* (Springer Berlin Heidelberg, Berlin, Heidelberg, 1999).
- [3] P. Y. Yu and M. Cardona, *Fundamentals of Semiconductors* (Springer Berlin Heidelberg, Berlin, Heidelberg, 2010).
- [4] M. B. Price, J. Butkus, T. C. Jellicoe, A. Sadhanala, A. Briane, J. E. Halpert, K. Broch, J. M. Hodgkiss, R. H. Friend, and F. Deschler, *Nat. Commun.* **6**, 8420 (2015).
- [5] J. M. Richter, F. Branchi, F. Valduga de Almeida Camargo, B. Zhao, R. H. Friend, G. Cerullo, and F. Deschler, *Nat. Commun.* **8**, 376 (2017).
- [6] F. Zheng, L. Z. Tan, S. Liu, and A. M. Rappe, *Nano Lett.* **15**, 7794 (2015).
- [7] P. Azarhoosh, S. McKechnie, J. M. Frost, A. Walsh, and M. van Schilfgaarde, *APL Mater.* **4**, 91501 (2016).
- [8] A. Miyata, A. Mitioglu, P. Plochocka, O. Portugall, J. T.-W. Wang, S. D. Stranks, H. J. Snaith, and R. J. Nicholas, *Nat. Phys.* **11**, 582 (2015).
- [9] K. Chen, J. K. Gallaher, A. J. Barker, and J. M. Hodgkiss, *J. Phys. Chem. Lett.* **5**, 1732 (2014).
- [10] R. O. Jones, Density functional theory: Its origins, rise to prominence, and future. *Rev. Mod. Phys.* **87**, 897 (2015).
- [11] P. E. Blöchl, Projector augmented-wave method. *Phys. Rev. B* **50**, 17953 (1994).
- [12] G. Kresse and J. Hafner, Ab initio molecular dynamics for liquid metals. *Phys. Rev. B* **47**, 558 (1993).
- [13] G. Kresse and J. Hafner, Ab initio molecular-dynamics simulation of the liquid-metal-amorphous-semiconductor transition in germanium. *Phys. Rev. B* **49**, 14251 (1994).
- [14] J. P. Perdew, K. Burke, and M. Ernzerhof, Generalized gradient approximation made simple. *Phys. Rev. Lett.* **77**, 3865 (1996).
- [15] D. D. Koelling and B. N. Harmon, A technique for relativistic spin-polarised calculations. *J. Phys. C* **10**, 3107 (1977).

- [16] K. Kunc and R. M. Martin, Ab initio force constants of GaAs: A new approach to calculation of phonons and dielectric properties. *Phys. Rev. Lett.* **48**, 406 (1982).
- [17] J. H. Lloyd-Williams and B. Monserrat, Lattice dynamics and electron-phonon coupling calculations using nondiagonal supercells. *Phys. Rev. B* **92**, 184301 (2015).
- [18] D. J. Hooton, The use of a model in anharmonic lattice dynamics. *Philos. Mag.* **3**, 49 (1958).
- [19] C. Motta, F. El-Mellouhi, S. Kais, N. Tabet, F. Alharbi, and S. Sanvito, Revealing the role of organic cations in hybrid halide perovskite CH₃NH₃PbI₃. *Nat. Commun.* **6**, 7026 (2015).
- [20] F. Zheng, L. Z. Tan, S. Liu, and A. M. Rappe, Rashba spin-orbit coupling enhanced carrier lifetime in CH₃NH₃PbI₃. *Nano Lett.* **15**, 7794 (2015).
- [21] T. Etienne, E. Mosconi, and F. De Angelis, Dynamical origin of the Rashba effect in organohalide lead perovskites: A key to suppressed carrier recombination in perovskite solar cells? *J. Phys. Chem. Lett.* **7**, 1638 (2016)
- [22] B. Monserrat and D. Vanderbilt, Temperature dependence of the bulk Rashba splitting in the bismuth tellurohalides. *Phys. Rev. Materials* **1**, 054201 (2017).
- [23] B. Monserrat and D. Vanderbilt, Phonon-assisted spin splitting in centrosymmetric crystals. arXiv:1711.06274